

JOURNAL OF THE AMERICAN CHEMICAL SOCIETY

Radical Cation Transport and Reaction in Triplex DNA: Long-Range Guanine Damage

Yongzhi Kan and Gary B. Schuster*

School of Chemistry and Biochemistry, Georgia Institute of Technology, Atlanta, Georgia, 30332-0440

Received July 30, 1999

Abstract: Radical cation injection, transport, and reaction in DNA structures containing a triplex region were examined. An anthraquinone-linked polypyrimidine oligonucleotide was designed to form a pyrimidine-purine \times pyrimidine ($Y \cdot R \times Y$) triplex. Spectroscopic and DNase I footprinting experiments verified triplex formation and indicated intercalation of the anthraquinone group at the triplex–duplex junction. Irradiation of the triplex at 350 nm (only the anthraquinone absorbs) leads to reactions at remote locations in both the duplex and triplex regions. These reactions are revealed as strand breaks by subsequent treatment of the irradiated samples with piperidine. Radical cations injected at the triplex–duplex junction migrate into and through the triplex region. The effect of cytosine protonation on radical cation migration and reaction was examined. These observations support the charge transport mechanism in DNA that we recently identified as phonon-assisted polaron hopping.

Introduction

Charge transport through DNA is a topic of substantial interest and possible importance. In particular, one-electron oxidation forms a radical cation that can migrate through both duplex DNA and single-stranded regions, causing damage (chemical reaction) selectively at guanines.^{1–5} Damaged guanines have been implicated as sources of mutation that can lead to disease and aging.^{6,7} Although it has been understood for some time that charge does migrate in DNA, the mechanism for charge transport was controversial.^{8,9} Also, there is growing interest

in the potential use of DNA as a one-dimensional quantum wire in mesoscopic devices. Measurements on desiccated “ropes” of DNA in a vacuum reveal its resistivity to be $\sim 1\text{ M}\Omega\text{ cm}$. There is no understanding of the mechanism for this conduction.¹⁰

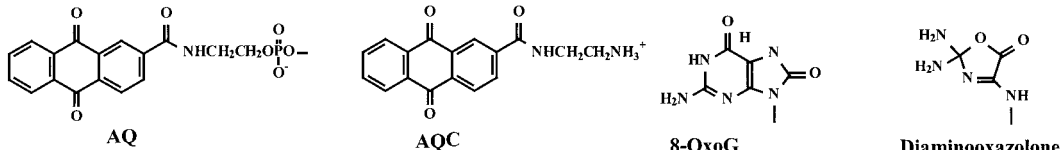
We have been examining DNA to assess the effect of its various structures on the injection, transport, and reactions of radical cations.^{11–13} This investigation led to a proposal for charge transport in A- and B-form DNA which we identify as phonon-assisted polaron-like hopping.⁸ In contrast, for single-stranded DNA the charge is transported by means of transient structures formed by guanine–guanine mispairs. The reactivity of radical cations in DNA depends on the structural form. In single strands, where the bases are exposed to solvent, deprotonation of the guanine radical cation and reaction of the resulting radical with O_2 leads, eventually, to its conversion

- (1) Arkin, M. R.; Stemp, E. D.; Pulver, S. C.; Barton, J. K. *Chem., Biol.* **1997**, *4*, 389–400.
- (2) Hall, D. B.; Holmlin, R. E.; Barton, J. K. *Nature* **1996**, *382*, 731–735.
- (3) Gasper, S. M.; Schuster, G. B. *J. Am. Chem. Soc.* **1997**, *119*, 12762–12771.
- (4) Nunez, M.; Hall, D. B.; Barton, J. K. *Chem., Biol.* **1999**, *6*, 85–97.
- (5) Meggers, E.; Michel-Beyerle, M. E.; Giese, B. *J. Am. Chem. Soc.* **1998**, *120*, 12950–12995.
- (6) Burrows, C. J.; Muller, J. G. *Chem. Rev.* **1998**, *98*, 1109–1154.
- (7) LePage, F.; Guy, A.; Cadet, J.; Sarasin, A.; Gentil, A. *Nucleic Acids Res.* **1998**, *26*, 1276–1281.
- (8) Henderson, P. T.; Jones, D.; Hampikian, G.; Kan, Y.; Schuster, G. B. *Proc. Natl. Acad. Sci. U.S.A.* **1999**, *96*, in press.

- (9) Wan, C.; Fiebig, T.; Kelley, S. O.; Treadway, C. R.; Barton, J. K.; Zewail, A. H. *Proc. Natl. Acad. Sci. U.S.A.* **1999**, *96*, 6014–6019.
- (10) Fink, H.-W.; Schronenberger, C. *Nature* **1999**, *398*, 407–500.
- (11) Armitage, B. A.; Yu, C.; Devadoss, C.; Schuster, G. B. *J. Am. Chem. Soc.* **1994**, *116*, 9847–9859.
- (12) Kan, Y.; Schuster, G. B. *J. Am. Chem. Soc.*, in press.
- (13) Sartor, V.; Henderson, P. T.; Schuster, G. B. *J. Am. Chem. Soc.*, in press.

Chart 1. Structures and DNA Oligonucleotides for Triplex Formation

AQ-14TC	5'-AQ T T T T T C C T T T T T -3'
DNA(1)	5'-G C T T A G G₁ T T A A A A A A G G₂ A A A A A A T T G G₃ A T T C G -3'
DNA(2)	3'-C G A A T C C A A T T T T T C C T T T T A A C C T A A G C -5'



primarily to diaminooxazolone (structures are shown in Chart 1).¹⁴ Deprotonation is slowed in B-form DNA by formation of the Watson–Crick hydrogen bonds. In this case, the radical cation is trapped predominantly at the 5'-G of GG steps by H₂O, resulting primarily in the formation of 7,8-dihydro-8-oxoguanine (8-OxoG).^{15,16} Guanine radical cations also react in the largely A-form helix of RNA/DNA hybrids. The efficiency of this process is less than it is in B-form DNA because reaction of H₂O is slowed by the more hydrophobic base stack of the A-form.¹³ We report here the extension of our investigation of radical cation transport and reaction to triple helical DNA.

DNA triple helices were first observed in 1957 for polyribonucleotides¹⁷ and then for polydeoxynucleotides and hybrids in 1968.^{18,19} Current interest in triplexes followed the discovery that sufficiently long stretches of purine-pyrimidine duplexes with mirror symmetry can disengage and then refold as a triple helix with an excluded pyrimidine single strand.^{20–23} Also, the sequence-specific association of an oligonucleotide probe to form a triplex with duplex DNA or messenger RNA has a variety of potential applications.^{24,25} Most relevant to the current work is the possible site-specific delivery of chemical functionality, such as nuclease activity, to a DNA duplex target.²⁶

Triplex formation most commonly relies on hydrogen-bonding interactions between bases in an oligopyrimidine strand with purines already engaged in Watson–Crick hydrogen bonding to pyrimidines.²⁷ Among the possible combinations, only two triplets T·A×T and C·G×C⁺ are isomorphous. This is the main reason triple helices preferentially form at homopurine-homopyrimidine (R×Y) sequences of DNA, and why triplex-forming oligonucleotides containing only pyrimidines (C and T) have been the major focus of recent studies. In an Y·R×Y

(14) Cadet, J.; Berger, M.; Buchko, G. W.; Joshi, P. C.; Raoul, S.; Ravanat, J.-L. *J. Am. Chem. Soc.* **1994**, *116*, 7403–7404.

(15) Kasai, H.; Yamaizumi, Z.; Berger, M.; Cadet, J. *J. Am. Chem. Soc.* **1992**, *114*, 1992.

(16) Angelov, D.; Spassky, A.; Berger, M.; Cadet, J. *J. Am. Chem. Soc.* **1997**, *119*, 11373–11380.

(17) Felsenfeld, G.; Davies, D. R.; Rich, A. *J. Am. Chem. Soc.* **1957**, *79*, 2023–2024.

(18) Riley, M.; Maling, B.; Chamberlin, M. *J. Mol. Biol.* **1966**, *20*, 359–389.

(19) Morgan, A. R.; Wells, R. D. *J. Mol. Biol.* **1968**, *37*, 63–80.

(20) Wells, R. D.; Collier, D. A.; Hanvey, J. C.; Shimizu, M.; Wohlrab, F. *FASEB J.* **1988**, *2*, 2939–2949.

(21) Hten, H.; Dahlberg, J. E. *Science* **1989**, *243*, 1571–1576.

(22) Lee, J. S.; Woodsworth, M. L.; Latimer, L. J. P.; Morgan, A. R. *Nucleic Acids Res.* **1984**, *12*, 6603–6614.

(23) Christophe, D.; Cabrer, B.; Bacolla, A.; Targovnik, H.; Pohl, V.; Vassart, G. *Nucleic Acids Res.* **1985**, *13*, 5127–5144.

(24) Moser, H. E.; Dervan, P. B. *Science* **1987**, *238*, 645–650.

(25) Francois, J. C.; Saison-Behmoaras, T.; Barbier, C.; Chassignol, M.; Thuong, N. T.; Helene, C. *Proc. Natl. Acad. Sci. U.S.A.* **1989**, *86*, 9702–9706.

(26) Armitage, B. *Chem. Rev.* **1998**, *98*, 1171–1200.

(27) Hoogsteen, K. *Acta Crystallogr.* **1959**, *12*, 822–823.

triplex, the oligopyrimidine third strand (Y) binds to the homopurine strand of the target DNA sequence in a parallel orientation.^{24,28–30}

In Y·R×Y Hoogsteen triplexes, cytosines provide maximum stability when they are protonated at N3, allowing a second hydrogen bond to be formed to the Watson–Crick guanine residue. This results in a pH dependence of the three-stranded complex's stability that is dependent on the population of third strand cytosines, as well as their positions relative to each other and relative to the ends of the third strand DNA.^{31–33} The pK_a of isolated deoxycytidine is ~4.3, but its apparent pK_a is raised in oligonucleotides and multistranded nucleic acids presumably due to their polyanionic character, hydrogen bonding of the proton to N7 of guanine and more favorable interactions between neighboring bases.^{32–35}

Structural studies of DNA triplexes have revealed that the third strand lies in the major groove of the duplex^{36,37} and that the duplex within the triplex is unwound relative to B-form DNA.^{38–40} NMR techniques are intensively used in the studies of triple-helical complexes.^{41–43} The deoxyribose conformation of all strands correspond to an S-type (C2'-endo) pucker. Significantly, Radhakrishnan and Patel⁴⁴ found that the interstrand and intrastrand overlap patterns exhibited by the aromatic heterocycles in the Watson–Crick duplex segment of Y·R×Y triplex are similar, although not identical to those found in A-form helices. These results indicate that the triplex conformation is not identical to either A- or B-form DNA.

(28) Le Doan, T.; Perrouault, L.; Praseuth, D.; Habhou, N.; Decout, J. L.; Thuong, N. T.; Lhomme, J.; Hélène, C. *Nucleic Acids Res.* **1987**, *15*, 7749–7760.

(29) Preseut, D.; Perrouault, L.; Le Doan, T.; Chassignol, M.; Thuong, N.; Hélène, C. *Proc. Natl. Acad. Sci. U.S.A.* **1988**, *85*, 1349–1353.

(30) Manzini, G.; Xodo, L. E.; Gasparotto, D.; Quadrifoglio, F.; van der Marel, G. A.; Boom, v. *J. Mol. Biol.* **1990**, *213*, 833–843.

(31) Plum, G. E.; Park, Y. W.; Singleton, S. F.; Dervan, P. B.; Breslauer, K. J. *Proc. Natl. Acad. Sci. U.S.A.* **1990**, *87*, 9436–9440.

(32) Plum, G. E.; Breslauer, K. J. *J. Mol. Biol.* **1995**, *248*, 679–695.

(33) Asensio, J. L.; Lane, A. N.; Dhesi, J.; Bergqvist, S.; Brown, T. J. *Mol. Biol.* **1998**, *275*, 811–822.

(34) Volker, J.; Klump, H. H. *Biochemistry* **1994**, *33*, 13502–13508.

(35) Gaffney, B. L.; Kung, P. P.; Wang, C.; Jones, R. A. *J. Am. Chem. Soc.* **1995**, *117*, 12281–12283.

(36) Johnston, B. H. *Science* **1988**, *241*, 1800–1804.

(37) Voloshin, O. N.; Mirkin, S. M.; Lyamichev, V. I.; Belotserkovskii, B. P.; Frank-Kamenetskii, M. D. *Nature* **1988**, *333*, 475–476.

(38) Lyamichev, V. I.; Mirkin, S. M.; Frank-Kamenetskii, M. D.; Cantor, C. R. *Nucleic Acids Res.* **1988**, *16*, 2165–2178.

(39) Arnott, S.; Selsing, E. *J. Mol. Biol.* **1974**, *88*, 509–521.

(40) Arnott, S.; Bond, P. J.; Selsing, E.; Smith, P. J. C. *Nucleic Acids Res.* **1976**, *2450*–2470.

(41) de los Santos, C.; Rosen, M.; Patel, D. *Biochemistry* **1989**, *28*, 7282–7289.

(42) Rajagopal, P.; Feig, J. *Nature* **1989**, *339*, 637–640.

(43) Pilch, D. S.; Levenson, C.; Shafer, R. H. *Proc. Natl. Acad. Sci. U.S.A.* **1990**, *87*, 1942–1946.

(44) Radhakrishnan, I.; Patel, D. J. *Structure* **1994**, *2*, 17–32.

Covalent attachment of various chemical functionalities to oligonucleotides that can form triple helices with target duplexes has been explored for a variety of purposes.^{45–54} We attached an anthraquinone group (AQ) through a four-atom tether to the 5'-end of an oligopyrimidine strand, AQ-14TC (Chart 1). This strand binds to its targeted duplex DNA, and irradiation of the anthraquinone results in radical cation injection. We studied the migration of this charge through the triplex and its reactions at GG steps in the triplex and duplex regions. Findings from this work expand the mechanistic understanding of charge transport and reaction in DNA.

Results

(1) Design and Characterization of AQ-Conjugated Triplex DNA. AQ-14TC is an oligonucleotide consisting entirely of pyrimidines with an anthraquinone group linked to its 5'-end. It was prepared by solid-phase synthetic methods, which have been previously described³ and was purified by HPLC. The base sequence of AQ-14TC was selected so that it would form an Y·R×Y parallel mode triplex with duplex DNA(2)·DNA(1). The triplex structure contains three 5'-GG-3' steps on DNA(1) that serve as indicators for radical cation migration and reaction. The first, GG₁, is in a duplex region identified as “upstream” from the AQ group. GG₂ is in the expected triplex region, and GG₃ is part of the duplex that is “downstream” of the AQ group. We carried out a series of experiments to assess the triplex structure.

(a) Melting-UV. The melting behavior of DNA is a diagnostic tool useful to evaluate the formation and stability of triplex structures. Duplex DNA(1)·DNA(2) was prepared by heating an equimolar phosphate buffer solution (pH = 6.2) of each strand to 90 °C and then slowly cooling the mixture to room temperature. A sample of AQ-14TC was added to the solution and then incubated at ~4 °C for 24 h. The triplex formed by this hybridization procedure was characterized by its melting behavior from 5 to 60 °C monitored at 260 nm by UV spectroscopy. The heating curves obtained for the DNA(2)·DNA(1)×AQ-14TC triplex, with and without added 10 mM MgSO₄, are shown in Figure 1.

The melting curves show two transitions (T_m), which is typical behavior for short oligonucleotide triplets. The lower T_m (18.5 °C without MgSO₄, 28.6 °C with it) is assigned to the dissociation of AQ-14TC from duplex DNA(2)·DNA(1), this is the so-called Hoogsteen transition (HG). The higher T_m , the Watson-Crick transition (WC), which characterizes the conversion of the duplex into single strands, occurs at 65 °C in the

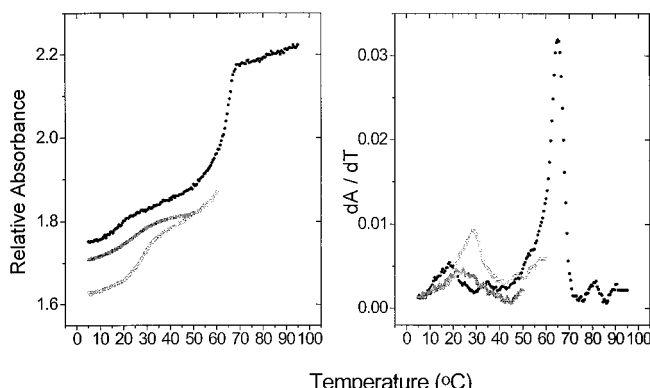


Figure 1. Heating curves obtained by monitoring the absorbance of the triplex in 10 mM NaPO₄ (pH 6.2) with increasing temperature are shown on the left. The corresponding first-derivative curves are shown on the right. Filled circle = DNA(2)·DNA(1)×AQ-14TC without MgSO₄ (T_m (HG) = 18.5 ± 0.5 °C); open circle = DNA(2)·DNA(1)×AQ-14TC with 10 mM MgSO₄ (T_m (HG) = 28.6 ± 0.5 °C); filled up triangle = DNA(2)·DNA(1) × 14TC with 10 mM MgSO₄ (T_m (HG) = 23.0 ± 0.5 °C).

absence of MgSO₄. The DNA precipitated at higher temperatures from samples containing Mg²⁺, consequently the T_m (WC) could not be measured for these solutions. Figure 1 also shows the melting curve for DNA(2)·DNA(1)×14TC, which has the same oligonucleotide sequences but does not have the AQ group. Its T_m (HG) is ~5 °C below that of the AQ-containing compound. These data indicate triplex formation and its stabilization by the covalently linked quinone. This is consistent with previous work, which showed that covalently linked intercalators attached to a triplex-forming strand stabilize the triplex and intercalate at the triplex–duplex junction.⁵⁵

(b) Melting-CD. Tuite and Nordén showed that duplex poly(dT·dA) and triplex poly(dT·dA×dT) exhibit characteristic circular dichroism (CD) spectra between 200 and 240 nm.⁵⁶ Figure 2A shows the CD spectrum of DNA(2)·DNA(1)×AQ-14TC recorded between 5 and 60 °C. The negative band at ~210 nm, which is characteristic of the triplex, is present at 5 °C and disappears as the temperature is raised. The CD spectrum at high temperature is essentially the same as it is for duplex DNA(2)·DNA(1). Figure 2B is the melting profile for DNA(2)·DNA(1)×AQ-14TC monitored by CD spectroscopy at 210 nm. It confirms that T_m = 28 °C is the HG transition of the triplex.

(c) Phosphorescence-pH Effect. The efficiency of phosphorescence quenching reliably distinguishes anthraquinone groups that are bound to DNA by intercalation from those that are groove bound.⁵⁷ Optical excitation of the AQ chromophore yields its triplet state rapidly with high efficiency ($\Phi_{isc} = 0.9$).⁵⁸ We measured the phosphorescence of AQ-14TC under a range of conditions to assess the position of the AQ in the triplex.

Figure 3A shows the phosphorescence spectrum of AQ-14TC at 77 K in a frozen ethylene glycol/buffer solution. The emission intensity is ~40% lower than for the standard anthraquinone model, AQC (see Chart 1), which reveals some quenching in the randomly coiled single strand. The quenching increases dramatically in the presence of DNA(2)·DNA(1) and, importantly, it is pH-dependent (Figure 3B). At low pH (<5.8), more

(45) Sessler, J. L.; Sansom, P. I.; Kral, V.; O'Conner, D.; Iverson, B. L. *J. Am. Chem. Soc.* **1996**, *118*, 12322–12330.

(46) Miller, P. S.; Bi, G. X.; Kipp, S. A.; Fok, V.; Delong, R. K. *Nucleic Acids Res.* **1996**, *24*, 730–736.

(47) Tung, C. H.; Breslauer, K. J.; Stein, S. *Bioconjugate Chem.* **1996**, *7*, 655–661.

(48) Ganesh, K. N.; Rajeev, K. G.; Pallan, P. S.; Rana, V. S.; Barawkar, D. A.; Kumar, V. A. *Nucleosides Nucleotides* **1997**, *16*, 1271–1278.

(49) Zhou, B. W.; Puga, E.; Sun, J. S.; Garestier, T.; Helene, C. *J. Am. Chem. Soc.* **1995**, *117*, 10425–10428.

(50) Lacoste, J.; Francois, J. C.; Helene, C. *Nucleic Acids Res.* **1997**, *25*, 1991–1998.

(51) Wei, Z. P.; Tung, C. H.; Zhu, T. M.; Dickerhof, W. A.; Breslaur, K. J.; Georgopoulos, D. E.; Leibowitz, M. J.; Stein, S. *Nucleic Acids Res.* **1996**, *24*, 655–661.

(52) Ellouze, C.; Piot, F.; Takashi, M. *J. Biochem.* **1997**, *121*, 521–526.

(53) Robles, J.; McLaughlin, L. W. *J. Am. Chem. Soc.* **1997**, *119*, 6014–6021.

(54) Mohammadi, S.; Slama-Schow, A.; Leger, G.; El Manouni, D.; Shchyolkina, A.; Leroux, Y.; Taillandier, E. *Biochemistry* **1997**, *36*, 14836–14844.

(55) Sun, J. S.; de Bizemont, T.; Duval-Valentin, C.; Montenay-Garestier, T.; Helene, C. *Proc. Natl. Acad. Sci. U.S.A.* **1991**.

(56) Tuite, E.; Nordén, B. *Bioorg. Med. Chem.* **1995**, *3*, 701–711.

(57) Breslin, D. T.; Yu, C.; Ly, D.; Schuster, G. B. *Biochemistry* **1997**, *36*, 10463–10473.

(58) Wilkinson, F. *J. Phys. Chem.* **1962**, *66*, 2569–2574.

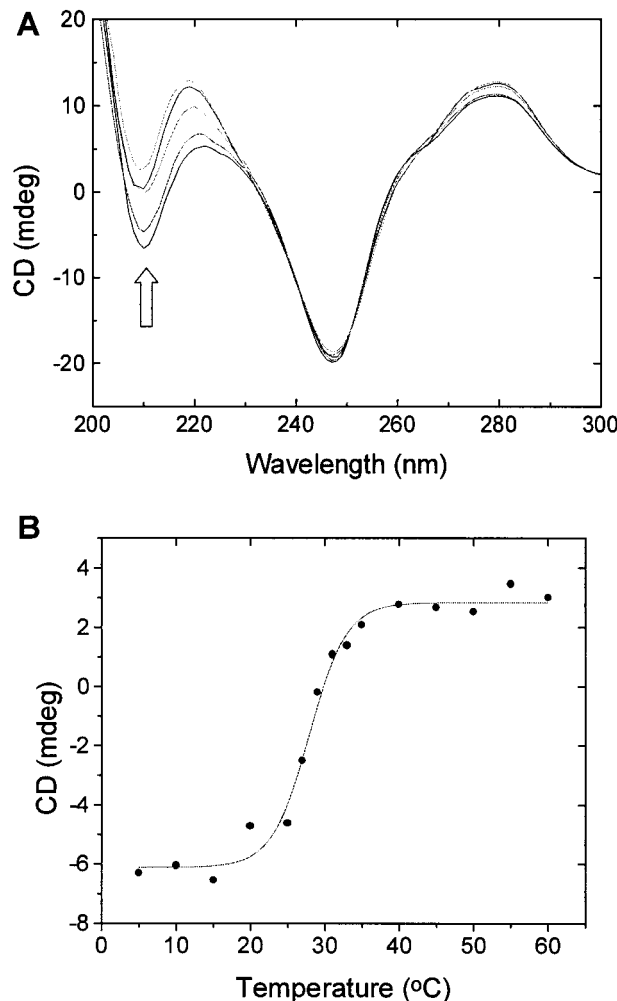


Figure 2. (A) CD spectra of the DNA(2)·DNA(1)×AQ-14TC triplex at temperatures from 5 to 60 °C. The spectra recorded at low temperature have a stronger band at ~210 nm (arrow), which is characteristic of triplex formation. (B) Triplex melting profile monitored with the temperature-dependent CD signals at 210 nm. The solid line is a fit to the data.

than 90% of the phosphorescence is quenched compared with AQ-14TC alone. The amount of quenching decreases as the pH of the solution is raised, and at high pH (>7.8) there is essentially no quenching by DNA(2)·DNA(1). The phosphorescence quenching experiments support triplex formation and suggest that the anthraquinone group is intercalated. The pH dependence is characteristic of Y·R×Y Hoogsteen triplets where protonation of cytosines increases stability.

(d) DNase I Footprinting. DNase I hydrolyzes duplex but not single strand or triplex DNA.⁵⁹ We used this selectivity to probe the structure of DNA(2)·DNA(1)×AQ-14TC. In these experiments, AQ-14TC was added to solutions (100 mM NaClO₄, 10 mM MgSO₄, pH = 6.2) of DNA(2)·(3'-³²P)DNA(1) and then equilibrated at ~5 °C for 24 h. The results of DNase I footprinting at 5 °C are shown in Figure 4, in lanes 1–8.

Three structures can be formed in solutions of AQ-14TC, DNA(1), and DNA(2) depending on concentration and equilibrium constants: duplex DNA(2)·DNA(1); duplex AQ-14TC·DNA(1); and triplex DNA(2)·DNA(1)×AQ-14TC. Figure 4, lanes 3–6, show the results of DNase I treatment for solutions of DNA(2)·DNA(1) containing no AQ-14TC, and those containing 1, 2, and 4 equiv, respectively. Lanes 1 and 2 are from

controls containing only DNA(1) and DNA(1) + AQ-14TC. Lanes 5 and 6 reveal unambiguous evidence for triplex formation, the footprint of the AQ-14TC strand is clearly visible. At the lower AQ-14TC concentration, lane 4, the triplex is only partially formed (~60%). A similar result is obtained by varying the concentration of DNA(2)·DNA(1), lanes 7–8. However, these experiments are less sensitive due to dilution of the ³²P-label.

The footprinting experiments produced an additional interesting result. As expected, DNase I does not hydrolyze the single strand of DNA(1) (Figure 4, lane 1). Lane 2 shows that a partial duplex is formed by AQ-14TC·DNA(1). The two strands in this structure are antiparallel. This orientation is opposite to that expected for the triplex, and it places GG₂ in the duplex region and both GG₁ and GG₃ in single strand overhangs. These structural features are revealed again by the photochemistry of these compounds.

(2) Photochemistry—Radical Cation Injection, Migration, and Reaction. We have discovered that electronically excited anthraquinones react with DNA either by hydrogen atom abstraction or by electron transfer depending on whether the quinone is bound in a groove or intercalated.^{57,60} Damage from hydrogen atom abstraction is nonselective, but electron transfer forms a radical cation, which migrates in duplex DNA and reacts primarily at the 5'-G of GG steps.^{2,11,61,62} This reaction is revealed by strand cleavage following piperidine treatment.^{63,64} We examined the light-induced reactions of triplex DNA(2)·DNA(1)×AQ-14TC under precisely the same conditions used for the DNase I footprinting experiments. The results are shown in Figure 4, lanes 9–16.

Irradiation of DNA(2)·DNA(1)×AQ-14TC for 1 h at 350 nm, where only the anthraquinone group absorbs, leads to piperidine-requiring strand cleavage in DNA(1) (Figure 4, lanes 12–14). Four cleavage sites are observed: two are at the 5'-G of GG₁ and GG₃; the third is the 3'-G of the 5'-GG₂A-3' sequence in the triplex region; and, the fourth is the A at the triplex–duplex junction proximal to GG₁. GG₃ is cleaved most efficiently, and both GG₁ and GG₂ are at least 10-fold less reactive. This pattern is notably different from that of duplex DNA.

Cleavage of the A at the triplex–duplex junction defines the location of the AQ group and supports assignment of the expected parallel orientation for AQ-14TC in the triplex. Comparison with the results from irradiation of the partial duplex, AQ-14TC·DNA(1), Figure 4, lane 10, is particularly striking. In this case, strand cleavage occurs mostly at GG₂ in the duplex region, with less efficient cleavage at both the 5'- and 3'-G of GG₁ and GG₃ in the single strand overhang. This pattern of reactivity is characteristic of other partial duplexes we have investigated.¹²

Since the anthraquinone group in AQ-14TC is covalently linked with a four-atom tether, direct contact with the GG steps of DNA(1) in the triplex is prohibited. Consequently, radical cation migration is required if reaction at the remote guanines is intramolecular. We carried out control experiments to search for a possible intermolecular component. In particular, irradiation of mixtures containing a ³²P-labeled oligonucleotide, non-

(60) Henderson, P. T.; Armitage, B.; Schuster, G. B. *Biochemistry* **1998**, 37, 2991–3001.

(61) Ito, K.; Inoue, S.; Yamamoto, K.; Kawashita, S. *J. Biol. Chem.* **1993**, 268, 13221–13227.

(62) Saito, I.; Takayama, M.; Sugiyama, H.; Nakatani, K.; Tsuchida, A.; Yamamoto, M. *J. Am. Chem. Soc.* **1995**, 117, 6406–6407.

(63) Ly, D.; Kan, Y.; Armitage, B.; Schuster, G. B. *J. Am. Chem. Soc.* **1996**, 118, 8747–8748.

(64) Breslin, D. T.; Schuster, G. B. *J. Am. Chem. Soc.* **1996**, 118, 2311–2319.

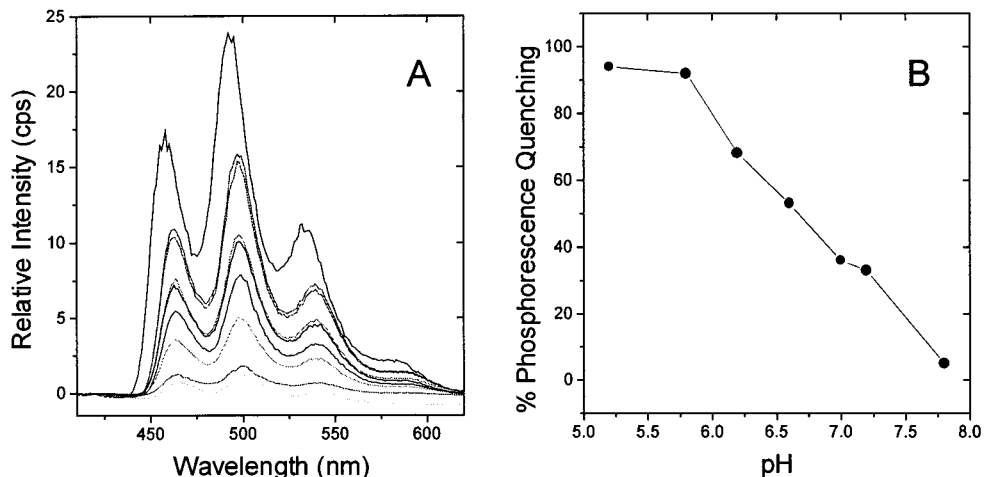


Figure 3. (A) Phosphorescence emission of anthraquinone in a frozen ethylene glycol-containing glass at 77 K (from top to bottom): free AQ, AQ-14TC, DNA(2)·DNA(1)×AQ-14TC (pH = 7.8, 7.2, 7.0, 6.6, 6.2, 5.8, 5.2). (B) Phosphorescence quenching of anthraquinone in DNA(2)·DNA(1)×AQ-14TC at various pHs.

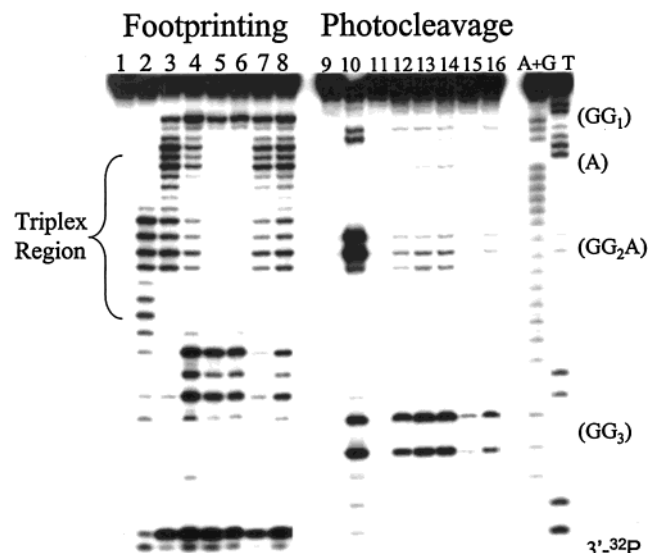


Figure 4. Footprinting with DNase I and photocleavage of triplex DNA(2)·(3'-³²P)DNA(1)×AQ-14TC: lanes 1–8, DNase I footprinting. In lanes 9–16, the samples were irradiated for 1 h at 350 nm and then treated with piperidine for 30 min at 90 °C. Lane 1: DNA(1). Lane 2: DNA(1) + AQ-14TC. Lane 3: DNA(1) + DNA(2). Lane 4: DNA(1) + DNA(2) + AQ-14TC (1 equiv of each strand). Lane 5: DNA(1) + DNA(2) + AQ-14TC (1:1:2 equiv, respectively). Lane 6: DNA(1) + DNA(2) + AQ-14TC (1:1:4 equiv, respectively). Lane 7: DNA(1) + DNA(2) + AQ-14TC (4:4:1 equiv, respectively). Lane 8: DNA(1) + DNA(2) + AQ-14TC (2:2:1 equiv, respectively). Lane 9: DNA(1). Lane 10: DNA(1) + AQ-14TC. Lane 11: DNA(1) + DNA(2). Lane 12: DNA(1) + DNA(2) + AQ-14TC (1 equiv of each strand). Lane 13: DNA(1) + DNA(2) + AQ-14TC (1:1:2 equiv, respectively). Lane 14: DNA(1) + DNA(2) + AQ-14TC (1:1:4 equiv, respectively). Lane 15: DNA(1) + DNA(2) + AQ-14TC (4:4:1 equiv, respectively). Lane 16: DNA(1) + DNA(2) + AQ-14TC (2:2:1 equiv, respectively). The lanes labeled A+G and T are sequencing experiments.

complementary to AQ-14TC, mixed with AQ-14TC, either as a single strand or as a duplex (prehybridized with its own complement) does not lead to detectable cleavage in the noncomplementary oligonucleotide. This result eliminates the possibility that the AQ group of AQ-14TC, either as a single strand or when bound to duplex, could intercalate into another DNA molecule and cause reaction at guanine. Another possible intermolecular reaction, formation of singlet oxygen ($^1\text{O}_2$),⁶⁵ was tested by control experiments in D_2O solution. The lifetime of

$^1\text{O}_2$ increases \sim 10-fold when the reaction solvent is changed from H_2O to D_2O .⁶⁶ This effect has been used to verify the participation of $^1\text{O}_2$ in reactions with DNA since the increase in lifetime is manifested as more efficient reaction.⁶⁷ There is no measurable effect on the cleavage efficiency observed for irradiation of DNA(2)·DNA(1)×AQ-14TC in either H_2O or D_2O . This result eliminates $^1\text{O}_2$ as the cause of the long-range damage.

These experiments show that the reaction observed at the GG steps from irradiation of DNA(1)·DNA(2)×AQ-14T is intramolecular. The reactive species is a radical cation that migrates through the triplex DNA and reacts at the GG sites. This is a significant result since the distances from the anthraquinone group to the 5'-G of the GG steps vary considerably. GG₃ is the farthest away at \sim 57 Å, and it is separated from the AQ by a triplex bridge, but it is cleaved most efficiently. We carried out experiments to explore the reason for this result.

(3) Effect of pH on DNA(2)·DNA(1)×AQ-14TC. Under acidic conditions, triplets containing C·G×C⁺ triplets are more stable than those with only T·A×T triplets. One reason is that protonation of cytosine provides for a second hydrogen bond. A second is electrostatic attraction between the positively charged cytosine and the negatively charged nucleic acid backbone. Radical cation migration and reaction in C⁺-containing triplets might be controlled by the same factors. We studied the effect of pH on DNA(2)·DNA(1)×AQ-14TC to examine this possibility.

Figure 5 shows the effect of changing the pH from 7.0 to 5.2 on DNase I hydrolysis (lanes 1–5) and on the photochemistry of labeled DNA(2)·5'-³²P DNA(1)×AQ-14TC (lanes 6–10). As expected, reducing the pH favors formation of the triplex. The clear footprints of AQ-14TC that are seen at pH 5.2 and 5.8 (lanes 2 and 3) begin to diminish when the pH is increased from 6.2 to 7.0 (lanes 4 and 5). This indicates that the pK of cytosine in this sequence is greater than 5.2.

Irradiation of these samples at 350 nm leads to remote reactions revealed as strand cleavage following piperidine treatment (Figure 5, lanes 6–10). Quantitative comparisons of the cleavage efficiency from three independent sets of experi-

(65) Devasagayam, T. P. A.; Steenken, S.; Obendorf, M. S. W.; Schulz, W. A.; Sies, H. *Biochemistry* **1991**, *30*, 6283–6289.

(66) Rogers, M. A. J.; Snowden, P. T. *J. Am. Chem. Soc.* **1982**, *104*, 5541–5543.

(67) Showen, K. B.; Showen, R. L. *Solvent Isotope Effects on Enzyme Systems*; Academic Press: New York, 1982; Vol. 87.

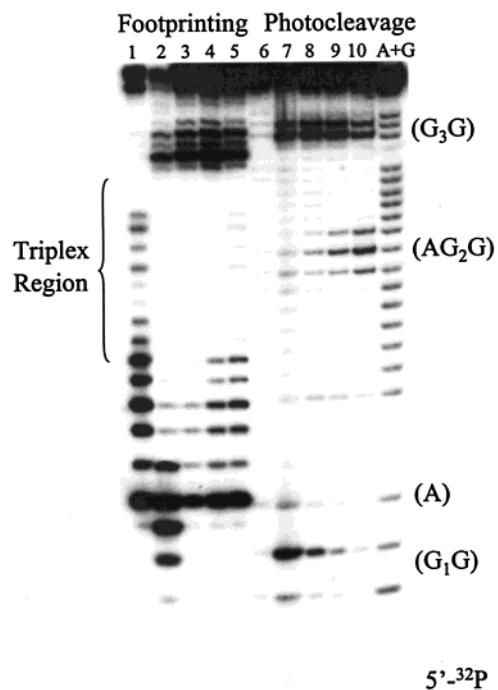


Figure 5. DNase I footprinting of the triplex DNA(2)·(5'-³²P) DNA(1)×AQ-14TC carried out at various pH values: lanes 1–5. Photocleavage of DNA(2)·(5'-³²P) DNA(1)×AQ-14TC (lanes 6–10) irradiated with 350 nm lamps for 1 h, and then treated with hot piperidine. Lane 1: DNA(1) + DNA(2). Lane 2: DNA(1) + DNA(2) + AQ-14TC at pH = 5.2. Lane 3: DNA(1) + DNA(2) + AQ-14TC at pH = 5.8. Lane 4: DNA(1) + DNA(2) + AQ-14TC at pH = 6.2. Lane 5: DNA(1) + DNA(2) + AQ-14TC at pH = 7.0. Lane 6: DNA(1) + DNA(2). Lane 7: DNA(1) + DNA(2) + AQ-14TC at pH = 5.2. Lane 8: DNA(1) + DNA(2) + AQ-14TC at pH = 5.8. Lane 9: DNA(1) + DNA(2) + AQ-14TC at pH = 6.2. Lane 10: DNA(1) + DNA(2) + AQ-14TC at pH = 7.0.

ments conducted from pH 5.2 to 7.8 are presented graphically in Figure 6A. The overall cleavage efficiency increases as the pH decreases. At pH 7.8, very little cleavage, or footprinting, is detected, which is an indication that little triplex is present. However, the total cleavage efficiency continues to increase on going from pH 5.2 to 5.8 although the footprinting experiments indicate that triplex formation is complete at the higher pH. Moreover, the three primary cleavage sites respond differently to the change in pH. These results suggest that the total cleavage efficiency is not determined solely by the amount of triplex formed.

The cleavage efficiency at GG₃ (in the downstream duplex) increases as the pH is lowered, but reaches a plateau at pH 5.8. This behavior parallels the pH dependence of triplex formation that is also revealed by the DNase I footprinting and phosphorescence quenching experiments. The cleavage efficiency at GG₂A (in the triplex) is more complex. It increases as the pH is reduced from 7.8 to 7.0, but then drops by nearly half at pH 6.6 and does not increase at lower pH. The unique effect of pH on cleavage at GG₂A is revealed in Figure 6B where analysis of the ratio of cleavage at GG₂A to GG₃ eliminates the effect of the pH dependence of the triplex concentration. These experiments show that cleavage at GG₂A, in the triplex region, becomes more efficient as pH increases.

Discussion

(1) **Formation and Structure of the Anthraquinone-Conjugated DNA Triplex.** The phosphorescence quenching and DNase I footprinting experiments both show nearly complete

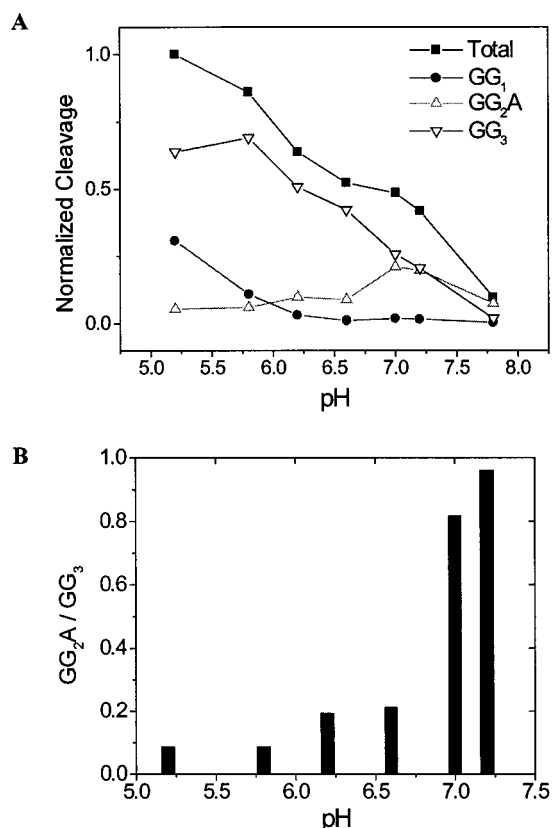


Figure 6. Quantification of the pH effect on photocleavage of DNA(1) + DNA(2) + AQ-14TC: (A) The effect of pH on the photocleavage at three GG steps. The data are the points, the lines connecting them are for clarity. (B) A bar graph representing the ratio of observed cleavage reaction efficiency at the GG₂A site to the amount measured at the GG₃ site at various pH.

formation of the triplex at pH < 5.8. This finding suggests that p*K* of cytosines on the third strand of the triplex are significantly above 4.3, which is the value for isolated cytosine.⁶⁸ The structure of the triplex is further revealed by the light-induced cleavage at the A on the 5'-end of the triplex-forming sequence. This provides direct evidence that the pyrimidine-rich AQ-14TC strand lies parallel to the purine-rich strand of the duplex, which is consistent with the prediction for triplex-forming oligonucleotides containing only pyrimidines.

It is known that compounds that normally intercalate in duplex DNA, when covalently attached to either the 5'- or 3'-end of the third strand of a triplex, intercalate at the triplex–duplex junction.⁶⁹ Random intercalation, such as an intermolecular interaction through an extrahelical geometry of the intercalator, is restricted when the linking chain is short. The increase in thermal stability of the triplex when AQ is linked to the third strand is an indication of intercalation. Also, the observation of nearly complete phosphorescence quenching of the AQ-conjugated triplex supports intercalative binding of the anthraquinone group. Finally, the light-induced cleavage experiments show reactions at guanine that are characteristic of radical cations. Experiments with unlinked quinones show that this reaction occurs only when the AQ is intercalated; quinones that bind in the groove show little, if any, G-selective cleavage.⁷⁰

(68) Leroy, J. L.; Gehring, K.; Kettani, A.; Gueron, M. *Biochemistry* 1993, 32, 6019–6031.

(69) Helene, C.; Toulme, J. J. *Biochim. Biophys. Acta* 1990, 1049, 99–125.

(70) Breslin, D. T.; Coury, J. E.; Anderson, J. R.; McFail-Isom, L.; Kan, Y.; Williams, L. D.; Bottomley, L. A.; Schuster, G. B. *J. Am. Chem. Soc.* 1997, 119, 5043–5044.

When intercalated, the hydrophobic anthraquinone group is partially shielded from the aqueous solvent and electron donor (a DNA base)—acceptor (the anthraquinone group) interactions provide forces that favor intercalative binding.⁷¹

These experiments support a structural model for the DNA(2)•DNA(1)×AQ-14TC triplex. In this model, the AQ-14TC strand binds parallel to the purine strand of duplex DNA(2)•DNA(1) and the anthraquinone group is intercalated. Since the four-atom linking chain restricts the duplex region accessible to the anthraquinone, it is probably intercalated at the 5'-TA-3' step of DNA(1). The results of irradiation of DNA(2)•DNA(1)×AQ-14TC are readily understood with this model.

(2) Long-Range Damage at Guanines. The operation of a long-distance charge transport process as the cause of G cleavage in these experiments is confirmed by observations which indicate that damage is intramolecular and that it does not involve $^1\text{O}_2$. The observation of light-induced cleavage at GG₃ requires charge migration through 14 base triplets and 2 base pairs, a distance of ~ 57 Å. We have proposed phonon-assisted polaron-like hopping as a mechanism for long-range radical cation migration in DNA.⁸ That model can be applied to the results reported here.

The polaron is defined as a local structural distortion in the DNA that relieves electron deficiency by delocalizing the radical cation over several bases. The number of bases incorporated in the polaron depends on the specific sequence. Hopping, a thermally activated process, causes the polaron to migrate. The hop length also depends on the specific sequence. The rate for polaron hopping (symbolized with k_h) is presumed to become averaged to a nearly constant value by variation of the number of bases in the polaron and by variation of the number of bases in a hopping step. In a simplified kinetic scheme, the polaron can hop, be annihilated (k_a), or be trapped (k_t). Annihilation is a process that consumes the polaron but does not give strand cleavage; trapping is a reaction of the polaron that results in strand cleavage. We interpret the results of charge injection into triplex DNA(2)•DNA(1)×AQ-14TC as being controlled by the relative magnitudes of these rates.

A key finding from these experiments is that the radical cation can migrate through the triplex region of DNA(2)•DNA(1)×AQ-14TC into the downstream duplex and cause reaction at GG₂ and GG₃. Evidently, base triplets do not prevent radical cation transport. However, it is likely that the magnitude of k_h is different in the duplex and triplex regions of DNA. Moreover, since protonation of cytosine in the C•G×C⁺ triplets introduces a positive charge in the radical cation migration path, this rate constant should depend on pH. This point will be discussed more fully below. Trapping of the radical cation involves its reaction with O₂ or H₂O.^{6,14,15} If a GG step is shielded from solvent, the trapping rate will be reduced. Formation of the triplex and cytosine protonation will affect the trapping rate.

Giese and co-workers have identified a possible charge transport mechanism in duplex DNA where radical cations move from G to G and runs of A and T are significant barriers.⁵ We have not observed this effect in duplex DNA systems,^{3,8} and runs of A and T are not significant barriers in the triplex region of DNA(2)•DNA(1)×AQ-14TC. In particular, a radical cation injected at the AQ intercalation site must pass through an (A)₆ sequence to reach GG₂ and then through a second (A)₆ sequence to reach GG₃. GG₃ is the site of most efficient reaction. The differences between our findings and those of Giese may be

due to variation in k_t and k_a . The chemical system they use to inject the radical cation introduces a strand break (nick), and this may affect the trapping and annihilation rates.

The results in Figure 5 show that irradiation of DNA(2)•DNA(1)×AQ-14TC gives nearly equal cleavage efficiencies for the GG₂ and GG₃ sites at pH ~ 7 (also see Figure 6). In duplex DNA it has been widely observed that radical cations cause reaction at the 5'-G of GG steps more efficiently.^{2,61–63} This 5'-selectivity has been attributed to either localization of charge density on the 5'-G^{72,73} or to a lowered activation barrier for reaction due to structural factors.⁷⁴ A major difference in the triplex region is that the 3'-G₂, which is between the 5'-G and a 3'-A, reacts most efficiently. The GGA site has been identified as one of relatively low oxidation potential.⁷² Three factors may contribute to the unique behavior in the triplex region.

One possibility is that the local conformation can affect the oxidation potential and localization of charge at a GG step.^{73,75} Structural studies indicate that the triplex conformation is not identical to either A- or B-form DNA.⁴⁴ In particular, overlap of the aromatic heterocycles in the Watson–Crick duplex segment of the triplex is different from a B-form helix. The changed electronic overlap of the bases in the triplex region might cause the site of positive charge localization to shift from the 5'-G to the 3'-G. Second, enhanced 3'-reactivity could be a direct consequence of triplex formation. A third groove is created in the triplex when the third strand occupies the major groove of duplex DNA. The GG step of the triplex is more hydrophobic because association of the third strand requires dehydration and release of counterions in the major groove.⁷⁶ However, recent studies reveal that the three triplex grooves each contain long-resident water spines.⁷⁵ Thus, the unique reaction selectivity at the triplex GG step may be determined by the access of these water molecules to the radical cation. Third, the properties of DNA(2)•DNA(1)×AQ-14TC are pH-dependent because formation of two Hoogsteen bonds in C•G×C⁺ triplets requires protonation of cytosine. Protonation at cytosine will result in positive charge at its paired guanine due to polarization effects and shifts in the position of protons in hydrogen bonds. Increased positive charge at G in the triplex could affect the efficiency of reaction at the GG₂ site. Thus, the shift away from 5'-G selective reaction in the triplex may be due either to a different site for charge localization caused by a change in overlap, a change in solvent accessibility, or an increased positive charge caused by C protonation.

Cytosine protonation in the triplex may also impact charge transport. The radical cation introduced at the AQ intercalation site must pass through C•G×C⁺ triplets to reach GG₃. The positive charge on or near these guanines could raise their oxidation potential and cause them to act as a barrier (decrease k_h) to polaron hopping. However, the data in Figure 6A indicate that the reaction at GG₃ is controlled primarily by the effect of pH on triplex formation. The efficiency of cleavage at GG₃ follows that for the formation of the triplex from pH 7.8 to 6.0. Below pH 6.0, the cleavage efficiency levels off, and this may be an effect of protonation on charge transport, but it is relatively small. A more significant effect of protonation is seen in the ratio of cleavage at GG₂ to GG₃, Figure 6B. These data show

(72) Saito, I.; Nakamura, T.; Nakatani, K.; Yoshioka, Y.; Yamaguchi, K.; Sugiyama, H. *J. Am. Chem. Soc.* **1998**, *120*, 12686–12687.

(73) Prat, F.; Houk, K. N.; Foote, C. S. *J. Am. Chem. Soc.* **1998**, *120*, 845–846.

(74) Gasper, S. M.; Armitage, B.; Hu, G. G.; Shui, X.; Yu, C.; Williams, L. D.; Schuster, G. B. *J. Am. Chem. Soc.* **1998**, *120*, 12402–12409.

(75) Fang, Y.; Wei, Y.; Bai, C.; Tang, Y.; Lin, S. B.; Kan, L. S. *Biomol. Struct. Dyn.* **1997**, *14*, 485–493.

(76) Chan, P. P.; Glazer, P. M. *J. Mol. Med.* **1997**, *75*, 267–282.

that reaction efficiency in the triplex region decreases strongly on cytosine protonation. This could be due to structural or electronic factors that change k_h or k_a .

Finally, the data in Figure 6 show that cleavage at GG₁ is much less efficient than it is at GG₃, although the former is closer to the site of charge injection. Reaction at GG₁, upstream of the intercalation site, may be controlled by local structural changes of the DNA such as unwinding at the triplex–duplex junction. Recent NMR study of an internally linked quinone revealed nonstandard B-DNA conformations.⁷⁷ We have observed⁷⁸ that intercalation of an anthraquinone in an internal position introduces structural changes that control radical cation migration and reaction. This same phenomenon may account for the reduced reactivity at GG₁ of the triplex.

Conclusions

These experiments reveal important structural and charge transport features of triplex DNA that are applicable to their use as site-selective photonucleases and which may provide some insight into the conductivity of desiccated DNA ropes. The results show clearly that the AQ-containing homopyrimidine third strand binds parallel to the purine strand of the targeted duplex. The evidence supports intercalation of the anthraquinone group at the duplex triplex junction. Irradiation of the AQ injects a radical cation, which can migrate through the triplex bridge into the downstream duplex. The radical cation causes reaction at GG steps which is revealed as strand cleavage after piperidine treatment. The reactivity pattern at the GG step is different in the triplex region than that which is seen universally in duplex DNA. In the duplex, the 5'-G of the GG step reacts more efficiently, in the triplex reaction at the 3'-G is more efficient. The properties of the triplex region are pH-dependent due to protonation of cytosine to form C•G×C⁺ triplets. Protonation does not appear to affect charge transport greatly, but it does inhibit trapping of the radical cation. The results of this investigation are interpreted within the kinetic scheme of the phonon-assisted polaron-hopping model. A major consequence of triplex formation is the reduction of reactivity of GG steps in the triplex region attributed to a decrease in k_t relative to k_h , which is associated with reduced access of H₂O to the radical cation in the triplex. Reduced H₂O reactivity may provide some insight into the observed conductivity of desiccated DNA. Radical cation migration through the triplex region to GG steps will limit the selectivity of photonucleases that rely on triplex formation for sequence recognition.

Experimental Section

Materials and Instrumentation. Radioactive isotopes [γ -³²P]-ATP were purchased from Amersham Bioscience. T4 Polynucleotide Kinase was purchased from Pharmacia Biotech and stored at -20 °C. Unmodified oligonucleotides (gel filtration grade) were obtained from the Midland Certified Reagent Company. 5'-End-linked anthraquinone oligonucleotides were synthesized as described elsewhere³ on an Applied Biosystems DNA synthesizer and were purified by reverse-phase HPLC. The extinction coefficients of the unmodified oligonucleotide were calculated using the nearest-neighbor values, and the absorbance was measured at 260 nm. Anthraquinone-modified oligonucleotide concentrations were determined in the same way as that of the unmodified oligomers except that an anthraquinone was replaced with adenine in the extinction coefficient determination. Ion-exchange and reverse-phase HPLC were performed on a Hitachi system using a

Vydac column. Matrix-assisted laser desorption ionization time-of-flight mass (MALDI-TOF) spectrometry of the conjugate strands was performed at the Midland Certified Reagent Company. UV melting and cooling curves were recorded on a Cary 1E spectrophotometer equipped with a multicell block, temperature controller, and sample transport accessory. CD spectra were recorded on Jasco-720 spectrometer.

UV Thermal Denaturation. Aqueous solutions were prepared containing 2 μ M of each oligonucleotide strand, with either 10 mM sodium phosphate buffer (pH varies from 5.8 to 7.0) or 10 mM sodium acetate buffer (pH 5.2) and 100 mM sodium perchlorate; 5–10 mM magnesium sulfate was added in some samples when specified. Melting curves (both heating and cooling) were obtained by monitoring the absorbance at 260 nm as the temperature was ramped from 0 to 60 °C or from 0 to 90 °C at a rate of 0.1 °C/min. First derivative curves were obtained from the original data for the melting temperatures.

Phosphorescence Quenching. Samples were prepared following the procedure in thermal denaturation experiment. Ethylene glycol (30% v/v) was added to each sample at ~5 °C. Phosphorescence emission spectra were recorded over the range 400–600 nm with the frozen glassy samples submerged in liquid nitrogen and excited at 330 nm. A blank sample containing only the ethylene glycol/buffer was used to record the baseline; subtraction of the blank spectrum eliminates light scattering effects at short wavelength.

Radiolabeling and Hybridization of Oligonucleotides. DNA oligomers were radiolabeled at the 5'-end with [γ -³²P] ATP and bacterial T₄ Polynucleotide Kinase.⁷⁹ The labeled DNA was purified by 20% PAGE. Stock solutions of complementary oligonucleotides were hybridized in 50 μ L of 10 mM sodium phosphate or sodium acetate (pH varies from 5.2 to 7.8) containing 100 mM sodium perchlorate, 10 mM magnesium sulfate when specified, 10 μ M each strand, and 10 000 cpm ³²P-labeled strand. The solutions were heated at 90 °C for 3 min and then allowed to cool to room temperature over a period of 2 h.

Triplex formation was accomplished by incubation of the DNA duplex (5 μ M) with the triplex-forming oligonucleotides (from 5 to 20 μ M) in a reaction mixture (40 μ L, one half for the DNase I assay, the other half for the photocleavage experiment), containing 10 mM sodium phosphate or sodium acetate (pH varies from 5.2 to 7.8), 100 mM sodium perchlorate, 10 mM magnesium sulfate when specified, at 4 °C overnight.

DNase I Footprinting. A sample of 2.2 μ L 10 \times DNase I reaction buffer (200 mM pH 8.4 Tris-HCl, 20 mM MgCl₂ 500 mM KCl) was added to 20 μ L of preincubated 5 μ M duplex or triplex solution, DNase I (0.2 μ g/mL final concentration) was added at 5 °C and the digestion was stopped after 5 min by freezing at -80 °C in the presence of 5-fold excess of ethanol. After ethanol precipitation, the samples were lyophilized and dissolved in denaturing buffer, the digests were separated on a 20% denaturing 19:1 acrylamide/bisacrylamide gel containing 7 M urea.

Cleavage Analysis by PAGE. Samples from the previous incubation were irradiated at 5 °C for 1 h in microcentrifuge tubes in a Rayonet Photoreactor (Southern New England Ultraviolet Company, Bransford, CT) equipped with 14 lamps (350 nm). After irradiation, the samples were precipitated once with ethanol, dried and treated with 1 M piperidine at 90 °C for 30 min. After evaporation of piperidine, drying, and suspension in denaturing loading buffer, samples (2500 cpm) were electrophoresed on a 20% denaturing 19:1 acrylamide/bisacrylamide gel containing 7 M urea. Gels were dried and the cleavage visualized by autoradiography.

Acknowledgment. This work was supported by grants from NSF and NIH, for which we are grateful.

JA992712Z

(77) Deshmukh, H.; Joglekarm, S. P.; Broom, A. D. *Bioconjugate Chem.* **1995**, 6, 578–586.

(78) Ly, D.; Sanni, L.; Schuster, G. B. *J. Am. Chem. Soc.* **1999**, 121, 9400–9410.

(79) Sambrook, J.; Fritsch, E. F.; Maniatis, T. *Molecular Cloning. A Laboratory Manual*, 2nd ed.; Cold Spring Harbor Press: Cold Spring Harbor, NY, 1989.